

博士論文

IMACEL : cell image analysis system revealed
stromule frequency at hourly intervals in Arabidopsis
stomatal guard cell chloroplasts.

(人工知能を活用した細胞画像解析システム IMACEL
の開発とストロミュールの形態解析)

島原 佑基

Acknowledgments

I first wish to express my most profound appreciation to Prof. Seiichiro Hasezawa (The University of Tokyo) for his guidance and encouragement throughout this study. I am also grateful to Dr. Natsumaro Kutsuna (The University of Tokyo) and Dr. Kei H. Kojo (Sophia University) for their instructions and critical suggestions and supporting my research. I thank Dr. Ko Sugawara(LPixel Inc.), and Dr. Hiroaki Kawai(LPixel Inc.) for development of IMACEL : cell image analysis system. I want to thank all of the members of the Laboratory of Plant Cell Biology in Totipotency for their help and encouragement. Finally, I want to thank my family and friends for their continuous support through this study. —

Contents

Acknowledgement	1
Contents	2
Abbreviation	6
General Introduction	8
Abstract	10
Chapter 1. Development of IMACEL: A cloud-based bioimage analysis platform for morphological analysis and image classification	12
Introduction	13
Methods	17
Implementation and architecture of the IMACEL platform	17
Security of the IMACEL platform	17
Cloud-based image processing	18
Interface of IMACEL with a click-based user interface	18
Classification algorithms in the IMACEL classifier	19
Cell culture of mammalian and plant cells	20
Stress treatment and immunofluorescence labelling	21
Microscope	21

Manual evaluation of the number and size	22
Statistical information	22
Result	22
Validation of the IMACEL particle analyser	23
Validation of the IMACEL classifier	24
Discussion	26
Figures	30
Figure 1. Architecture of IMACEL, a cloud-based image processing and machine learning platform for life science researchers.	30
Figure 2. Interface of the IMACEL particle analyser.	31
Figure 3. Results of the IMACEL particle analyser for extracting and evaluating stress granules in COS7 cells.	32
Figure 4. Results of the IMACEL classifier for cell cycle classification with nucleuses visualized using fluorescent images.	33
Supplemental Figure 1. Representative example of the manual evaluation of stress granules using ImageJ.	34
Supplemental Figure 2. Morphological analysis of stress granules using hierarchical clustering.	35

Supplemental Figure 3. Comparison of two different clusters generated by stress granules treated for 15 mins.	36
Supplemental Table 1 List of the implemented image processing methods in the IMACEL particle analyser.	37
Chapter 2. Quantitative evaluation of stomule frequency at hourly intervals in Arabidopsis stomatal guard cell chloroplasts	39
Introduction	40
Materials and Methods	42
Plant materials	43
Cell staining	43
Microscope	43
Quantitative evaluation of stomule frequency and statistical analysis	44
Result	45
Stomule frequency in light and dark conditions in Arabidopsis stomata	45
Detailed evaluation of stomule frequency at hourly intervals	46
Effect of lighting conditions on the periodic patterns of stomule frequency	47
Discussion	48
Detailed evaluation of stomule mean frequency at hourly intervals during the	

diurnal cycle	48
Synchronized and periodic patterns of stomule mean frequency in developing cotyledons	49
Stromule frequency in light and dark conditions	50
Roles of periodic patterns of stomule frequency	51
Figures	52
Figure 5. Representative images of chloroplasts with or without stromules and frequency of stromules in stomata of Arabidopsis seedlings of different ages.	52
Figure 6. Mean frequency of stromules in stomata during a diurnal cycle in Arabidopsis seedlings of different ages.	53
Figure 7. Mean frequency of stromules treated with 100 mM NaCl in stomata during a diurnal cycle in Arabidopsis seedlings.	54
Figure 8. Mean frequency of stromules in stomata of Arabidopsis seedlings grown under continuous light.	55
Conclusion	57
References	58

Abbreviation

2,4-D: 2,4-dichlorophenoxyacetic acid

BY-2: Bright Yellow 2

CaMV: Cauliflower mosaic virus

CCD: Colony Collapse Disorder

CO₂: Carbon Dioxide

COS: CV-1 (simian) in Origin, and carrying the SV40 genetic material

CPU: Central Processing Unit

CT: Computed Tomography

FM4-64:

N-(3-triethylammoniumpropyl)-4-(6-(4-(diethylamino)-phenyl)hexatrienyl)pyridinium

dibromide

FtsZ: Filamenting temperature-sensitive mutant Z

H2B: Histone 2B

MEM: Minimum Essential Medium

MRI: Magnetic Resonance Imaging

OpenCV : Open Source Computer Vision Library

PABP: Poly(A)-binding protein

PBS: Phosphate buffered salts

RAM: Random access memory

RFP: Red Fluorescent Protein

SDK: Software Development Kit

SSL: Secure Sockets Layer

TLS: Transport Layer Security

URL: Uniform Resource Locator

USDA: United States Department of Agriculture

YFP: yellow fluorescent protein

General Introduction

Life science as an academic field deals with enormous information. For instance, bioinformatics and bioimage informatics are disciplines in which information processing for life sciences is conducted, although the disciplines are still developing. The fields are highly influenced by advancement in computer and image processing technologies. Although large-scale information processing has increasingly become critical in biological research over the recent years, only a few biologists are conversant with the relevant information processing tools. In addition, since themes in biological research are diverse, it is necessary to develop software that are appropriate for respective research themes, which is a time consuming process. In the course of conducting research on cell physiology, I encountered a need to analyse large amounts of biological information from images, which could not be adequately achieved manually. Consequently, if systems that facilitate high-speed and high-precision analyses could be easily designed based on the respective target research activities, cell physiology research would advance more. Therefore, I embarked on developing a novel simple, high-speed, and high-accuracy cell image analysis system. In addition, I analysed a structure called stromule, whose roles in plant cells are largely unclear and has a complicated structure. The system developed through the present study could be employed by different researchers in

future, in addition to facilitating research on structures such as stromules.

Abstract

Automated quantitative image analysis is essential in research in all disciplines in the life sciences. Although numerous programs and algorithms have been developed for bioimage processing, an advanced understanding of image processing techniques and high-performance computing resources are required to apply them. Consequently, I developed a cloud-based image analysis platform called IMACEL, which integrates morphological analysis and machine learning-based image classification. The unique click-based user interface in IMACEL's morphological analysis platform provides researchers with resources for rapid and quantitative evaluation of elements without the need for prior knowledge of image processing. Since all the image processing and machine learning algorithms are implemented by high-performance virtual machines, users can access the same analytical environment from anywhere. A validation study of the morphological analysis and image classification of IMACEL was performed. The results indicate that the platform is an accessible and potentially powerful tool for the quantitative evaluation of bioimages, which could minimize the barriers in life science research. In chapter 1, I discuss the system.

In chapter 2, I analyse stromules, one of the organelles in the plant cell, using

IMACEL. Stromules are tubular structures that emerge from chloroplasts and other types of plastids. Although stromules have roles in plant immunity, little is known about other physiological functions of stromules or the significance of their formation, extent of protrusion, and frequency of occurrence. In the present study, I quantified the mean frequency of stromule occurrence in stomatal guard cells every hour during a diurnal cycle in developing and developed cotyledons in *Arabidopsis* seedlings. Stromule mean frequency was not constant during the diurnal cycle, but gradually increased and decreased, resulting in a local peak every 2–4 hours. Observations under continuous light revealed that the variation in stromule mean frequency was independent of the lighting conditions. The results provide novel information about stromule formation, revealing synchronized and periodic patterns of stromule frequency throughout the day–night cycle in guard cells of developing cotyledons.

Chapter 1

Development of IMACEL: A cloud-based bioimage analysis platform for morphological analysis and image classification

Introduction

Recent developments in microscopic and image processing technologies have led to new findings in the life sciences. With the evolution of imaging devices, such as microscopes, MRI, and CT, image data in the life sciences are increasingly detailed. In particular, the development of visualization techniques, such as the use of fluorescence microscopy and fluorescent probes, facilitate the analysis of biological structures and diversify molecular imaging. Therefore, it is becoming critical to analyse these bioimage data efficiently and quickly in quantitative studies (Peng *et al.* 2016, Danuser *et al.* 2011). Generally, the analysis of large and detailed images is very laborious and time-consuming, and is a burden for researchers. In addition to advances in imaging devices, a variety of open source and commercial image analysis software (e.g., ImageJ (Rueden *et al.* 2017), ImagePro, and Photoshop) and libraries for programming languages (e.g., OpenCV and Bioconductor) have been developed; however, their use requires specialist knowledge.

Machine learning is also used to analyse large quantities of bioimage data. Using this technique, it has become possible to automate or semi-automate analysis for the target extraction and classification of diverse and massive numbers of biological images (Sommer *et al.* 2013, Chang *et al.* 2011). Deep learning-based convolutional neural networks are expected to be useful for single-cell experiments with

high-throughput and high-content screening (Chessel *et al.* 2017, Kamatani *et al.* 2017). A report on using nonlinear dimensionality reduction in combination with deep learning to reconstruct cell cycle and disease progression has demonstrated the efficiency of applying machine learning techniques to objective biological prediction (Eulenberg *et al.* 2017). For instance, I previously proposed a system that combines machine learning and active learning (Settles *et al.* 2009) for subcellular localization, mitotic phase classification, and the discrimination of apoptosis in images of plant and human cells. This system achieved an accuracy level greater than or equal to that of the annotators (Kutsuna *et al.* 2012).

Although advanced image processing and machine learning techniques are necessary in life science studies, many research labs are ill-equipped to perform bioimage analysis that uses advanced imaging technologies and many computing resources. For generic morphological analysis, such as counting a number, measuring an area, and extracting several features of a shape, researchers need information about the signal/background setting, noise reduction filtering, binarization setting, and particle analyser function in de facto-standard image processing software ImageJ, and must manually choose particular algorithms for each specific research purpose and tune the parameters manually. Additionally, for classification analysis,

almost all software and analytical environments require skills for programming languages to input commands. Hence, although image processing plays an important role in quantitative data analysis for life sciences, the current available image processing solutions are too complicated for most researchers to use. Thus, user-friendly software for image analysis is needed to expand the use of imaging technologies throughout the life sciences.

IMACEL is a cloud-based image analysis platform developed for automatic classification and morphological analysis. Because all image processing and machine learning are performed by virtual machines in the cloud, it is not necessary to set up powerful laboratory computers or workstations. IMACEL's target data includes various types of microscopic bioimages. The most important feature in IMACEL is the new user interface for researchers with limited knowledge of image processing. IMACEL suggests multiple candidates for morphological analysis, allows users to select the most efficiently processed images. This allows users to determine appropriate procedures quickly and easily. In addition to morphological analysis, IMACEL can perform automatic image classification from uploaded annotated images using random forests and a deep learning algorithm.

The contributions of this study are as follows:

- I present a tool that enables life science researchers with limited image processing experience and computing resources to automatically and quantitatively analyse microscopic image data.

- I verify the morphological analysis of the system by evaluating the number and size of stress granules in images using the batch process function. Moreover, I evaluate the classification analysis of cell cycle progression using machine learning techniques on the IMACEL platform.

The adoption of IMACEL in life science research has the potential to improve the quality and quantity of research, particularly for researchers who would not otherwise have the experience and resources to perform such investigations.

Methods

Implementation and architecture of the IMACEL platform

IMACEL is a cloud-based image processing platform that runs on Windows, Mac OS X, and Linux. The image processing core modules of IMACEL were developed using Python 3 and OpenCV, and computation is performed on a virtual machine using the Microsoft Azure service.

A virtual machine with the standard D2 v2 instance type (2 vCPU, 7 GB RAM) was used in this study. Azure Storage was used as the image storage server. To connect to the storage server from a web application server, the Azure Storage SDK for Python was used. The database and web server used URLs for their connections to the storage server.

Security of the IMACEL platform

IMACEL used SSL/TLS to establish a secure connection between the web browser, web server, application server, and storage server. To grant limited access to resources in the storage server, a shared access signatures (SAS) provided by Azure Storage was used.

Cloud-based image processing

To use IMACEL, researchers upload images to the web server through a web browser, and the images are processed by high-performance virtual machines running on the Microsoft Azure platform that are able to communicate with the system's database (Fig. 1). Processed image data are sent back to the researchers through the web browser. The maximum data size for uploading images depends on the type of web browser. For example, Internet Explorer 11 has a limitation of 4 GB for file uploading.

Interface of IMACEL with a click-based user interface

The IMACEL platform includes a novel click-based interface designed for researchers who have no advanced image processing knowledge (Fig. 2). Researchers can upload images to IMACEL, specifying the imaging method (e.g., fluorescence, bright field, or electron microscopy) and imaging target (e.g., bacteria, yeast, mammalian cells, or brain tissue) to enable the IMACEL particle analyser to provide practical suggestions (Fig. 2a). In the image processing procedure, users click on the most appropriate processed image shown in the browser (Fig. 2b). This clickable user interface allows researchers at all skill levels to extract particles

quantitatively and objectively from raw input images (Figs 2c, d).

Several watershed algorithms are available at the last stage of the procedure. Additionally, several morphological features of particles, such as a number, area, roundness, fitted ellipse long and short axes, centroid coordinates, and solidity, are extracted automatically.

The IMACEL platform is designed for scientific image processing with a focus on bioimaging. Hence, all suggested procedures are appropriate for maintaining bioimage integrity (Supplemental Table 1). To enable the archiving of image processing procedures in each researcher's experimental notes, an image processing report is also provided (Fig. 2e).

Classification algorithms in the IMACEL classifier

Two classification algorithms are implemented in the current version of IMACEL: a random forest and a deep learning algorithm. The convolutional neural network architecture of AlexNet, which was first place in the ImageNet Large Scale Visual Recognition Challenge 2012 (ILSVRC2012) (Krizhevsky *et al.* 2012), is used. AlexNet consists of eight layers: five convolutional layers and three fully connected layers. Moreover, the version used in IMACEL was pre-trained on the data used in

ILSVRC2012.

Cell culture of mammalian and plant cells

The tobacco (*Nicotiana tabacum*) BY-2 cell line was diluted 95-fold with a modified Linsmaier and Skoog medium supplemented with 2,4-D at weekly intervals, as previously described (Nagata *et al.* 1992) . The cells were agitated on a rotary shaker at 130 rpm at 27 °C in the dark. The cell cycle progression was synchronised with 5 mg aphidicolin (Sigma), as previously described (Nagata *et al.* 1992) . A transgenic BY-2 cell line, stably expressing an RFP-Histone H2B fusion protein, could be maintained and synchronised by procedures similar to those used for the original BY-2 cell line.

African green monkey kidney fibroblast-derived COS7 cells were obtained from the RIKEN BioResource Center and cultured in high glucose Dulbecco's modified Eagle's medium (Gibco) supplemented with 10% qualified heat inactivated fetal bovine serum from USDA-approved regions (Gibco), 50 U/mL penicillin-50 µg/mL streptomycin (Gibco), 2 mM L-glutamine (Gibco), 1 mM sodium pyruvate (Gibco), MEM nonessential amino acids (Gibco), and 55 µM 2-mercaptoethanol (Gibco) at 37 °C in 5% CO₂.

Stress treatment and immunofluorescence labelling

COS7 cells cultured onto a 35-mm glass-based dish (IWAKI) were treated with 0.5 μ M sodium arsenite (Fluka) for 15 min or 60 min and fixed with 3% paraformaldehyde (Sigma Aldrich) and 0.1% glutaraldehyde (Sigma Aldrich) at 37°C in 5% CO₂ for 10 min. COS7 cells were permeabilised with 0.2% Triton-X 100 (SIGMA) and blocked at 37°C in 5% CO₂ for 30 min with 10% goat serum (Life Technologies) and then incubated for 30 min with primary antibodies, rabbit polyclonal anti-PABP antibody (Abcam), diluted in Can Get Signal Solution A (TOYOBO). After washing with 0.2% Triton-X 100 and PBS, the cells were incubated with Alexa 488 labelled goat anti-rabbit secondary antibodies diluted in Can Get Signal Solution A.

Microscope

For the observation of the cell cycle in BY-2 cells, the cells were imaged using fluorescent microscopy (FSX100, Olympus, Tokyo, Japan). To extract the nuclear regions, the images were processed manually using ImageJ.

To observe the COS7 cells, they were imaged using fluorescence microscopy (N-STORM, Nikon, Tokyo, Japan). Noise in the fluorescent microscopy image was

reduced with a difference of Gaussian filter using ImageJ.

Manual evaluation of the number and size

To evaluate the number and size of stress granules, boundaries were traced manually using ImageJ software. Manual evaluations were performed by two researchers who were not involved in this study to avoid biases that could overestimate the differences in treatment effect and underestimate the differences between the results of the manual evaluation and IMACEL particle analyser.

Four experts in plant cell division annotated the training data for the classification of cell cycle progression in tobacco BY-2 suspension-cultured cells.

Statistical information

To evaluate the differences in the number of stress granules, the Mann–Whitney U test was calculated using free statistical software R and R Studio versions 3.3.1 and 1.1.383, respectively.

Results

As illustrated in Fig 1, IMACEL is a cloud-based image processing platform.

Researchers upload images to the web server through a web browser. Image processing and image classification are performed by high-performance virtual machines, and the processed image data are sent back through the web browser. IMACEL has the following two independent functions: a particle analyser for morphological analysis and a classifier for bioimage classification.

Validation of the IMACEL particle analyser

I validated the morphological analysis of the IMACEL particle analyser by determining how similar its extracted features were to those of a manual evaluation. I focused on immunologically labelled stress granules because the shapes of the organelles are oval and traced easily by manual evaluation (as shown in Supplemental Fig. 1). It has been reported that a treatment of sodium arsenite induces the development of stress granules in a time-dependent manner (Nover *et al.* 1989, Nover *et al.* 1983, Collier *et al.* 1986). Therefore, COS7 cells treated with 0.5 μ M sodium arsenite for 15 min and 60 min were analysed with respect to the size and number of stress granules formed during treatment. I confirmed that the stress granules were segmented appropriately by the IMACEL particle analyser (Fig 3a). As expected, there were significant differences in the number and size of stress granules

between the 15 min and 60 min treatments, and the morphological analysis of IMACEL yielded results that were very similar to those of the manual evaluation (Figs 3b, c). The batch process of the IMACEL particle analyser (65 images each for specimen treated for 15 min and 60 min) was finished in approximately 5 min. In contrast, manual evaluation by tracing each stress granule took approximately 16 h (Fig 3d). In addition, hierarchical clustering analysis revealed that the 15-min and 60-min treatments were different and that the 15-min treatment group could be further divided into 2 groups. Specifically, comparing the two groups within the 15-min treatment group revealed a significant difference in circularity, although there was no difference in area. It also suggested a physiological basis for the control of the circularity of the stress granules (Supplemental Fig. 2, 3). The results indicate that the IMACEL particle analyser can evaluate the morphology of particles, both quantitatively and rapidly, with high accuracy.

Validation of the IMACEL classifier

To validate the IMACEL classifier, a classification of cell cycle progression in tobacco BY-2 suspension-cultured cells was performed using two machine learning methods: random forests and deep learning. Because of its highly synchronized cell

cycle progression (Kumagai-Sano *et al.* 2006), this cell cycle is very suitable for bioimage classification (Fig. 4a). Moreover, synchronized BY-2 cells are one of the most suitable suspension-cultured cells for observing each cell cycle. Nucleuses and chromosomes were visualized using histone H2B-RFP (Kumagai-Sano *et al.* 2006, Hayashi *et al.* 2007), and the image features were extracted using the LPX296 feature extractor formerly the KBI feature extractor (Caplan *et al.* 2015) and a higher-order local autocorrelation feature extractor.

The classification dataset was composed of 1,619 images of seven classes (Fig. 4b). To avoid overfitting, the mean accuracy was calculated using three-fold cross-validation.

The random forest IMACEL classifier (Kutsuna *et al.* 2012) identified seven cell cycle classes with a mean accuracy of approximately 76.69% and four classes with a mean accuracy of approximately 83.31% (Fig. 4c). S/G2 and metaphase were classified with high accuracy, but pro-metaphase and anaphase were classified with comparatively low accuracy (Fig. 4d).

By contrast, the deep learning method in IMACEL managed to identify seven cell cycle classes with a mean accuracy of approximately 80.17% and four classes with a mean accuracy of approximately 86.21% (Fig. 4c). The mean accuracies of

pro-metaphase and anaphase classification increased when deep learning classification was used (Fig. 4d).

These results indicate that IMACEL can automatically classify images without requiring researchers to have advanced knowledge of various image processing and machine learning techniques.

Discussion

The development of the IMACEL platform was based on two design concepts. The first concept is that of a novel clickable-based user interface. Existing image processing software, such as ImageJ or Photoshop CC, requires researchers to actively select the desired function from a list of image processing procedures. Because there is so much flexibility in the function selection, mistakes can be made if inappropriate image processing procedures are used. For example, a nonlocal mean filter (Buades *et al.* 2005), which is an effective noise reduction method, performs smoothing using similar intensity distributions from distant regions independently of whether the regions are biologically identical or not. Therefore, when such filtering is implemented in image processing software, researchers should avoid using it. By contrast, the IMACEL particle analyser effectively restricts the functions that can be

selected by those unfamiliar with image processing. Additionally, batch processing is easily performed without the need to write macro functions in a programming language.

The second concept is that of a cloud-based image processing platform. Generally, machine learning requires extensive computing resources. The construction of an analytical environment is too complex for many biological researchers. Moreover, high-performance machines are expensive to establish in each laboratory. In IMACEL, because image processing and machine learning are performed on high-performance virtual machines, users can freely access their own analytical environment via a web browser from anywhere. Additionally, because IMACEL stores previous analytical images, the platform could play the role of an image management tool.

I developed this platform for researchers in the broad field of life sciences. Microscopic images are more often observed than MRI images in some life science journals. Therefore, I focused this validation study on (fluorescence) microscopic images. However, in a related study, a prototype version IMACEL was used to classify transmitted electron microscopic images of tumorigenic cancer stem cells into two categories (ABCGS2+ and ABCGS2-) (Sasaki *et al.* 2018) . However, on the IMACEL platform, I do not restrict the image acquisition tools or type of image that

may be used for analysis. In fact, I am developing an extension to the image processing platform that is focused on MRI, CT, and X-ray images for specific fields of life science.

Compared with manual labelling, the classification methods in IMACEL are not highly accurate. There are several reasons for this performance in this study. First, the number of images in my dataset was small, particularly for the anaphase cell images. Deep learning is well known to perform better with a large number of images, and if one class has few examples, the resulting dataset can be imbalanced and affect the accuracy. Second, each cell cycle image was acquired using cheap fluorescent microscopy instead of a more advanced method, such as confocal laser scanning microscopy, and high levels of image noise could affect the result. Third, transfer learning could have affected the result. AlexNet was trained using not only microscopic images but also general images. Note that the above poor study conditions were selected to assess the IMACEL platform because it is aimed at researchers who do not have advanced computing skills or equipment.

A current version of the IMACEL platform, all microscopic images used in this study and detailed documentations will be distributed to interested researchers on request. Currently, I am developing three-dimensional reconstruction and the extraction of the

surface area and volume for three-dimensional images. Additionally, tracking or kinetic analysis for time-sequential observations is under development.

In conclusion, I developed a new cloud-based image processing platform called IMACEL that consists of morphological analysis and image classification functions. The validation experiments indicate that particles can be extracted easily and rapidly with high accuracy. Additionally, IMACEL enables researchers to perform image classification based on machine learning without prior knowledge of image processing.

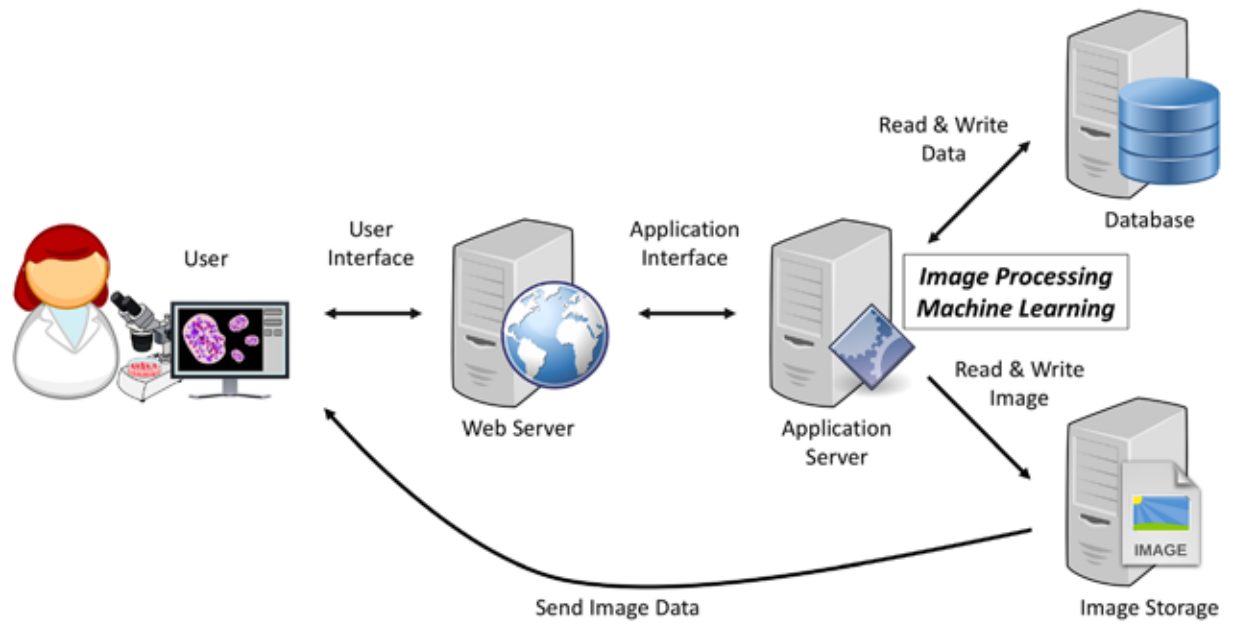


Figure 1. Architecture of IMACEL, a cloud-based image processing and machine learning platform for life science researchers.

The entire process of image processing is performed in the cloud using high-performance virtual machines. The public-domain images used in this figure were obtained from Openclipart.

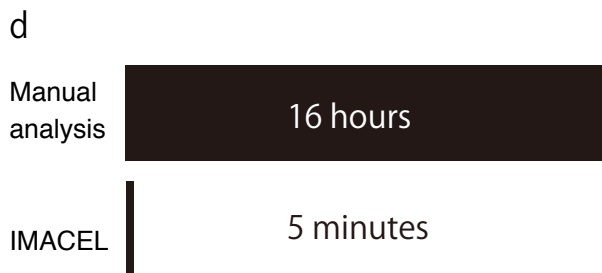
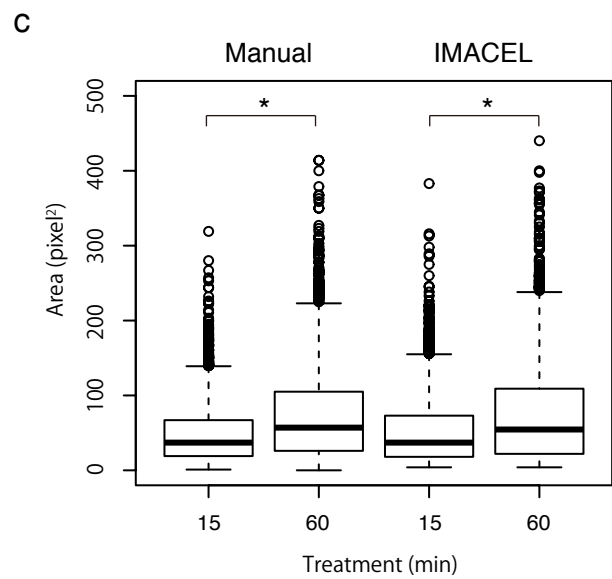
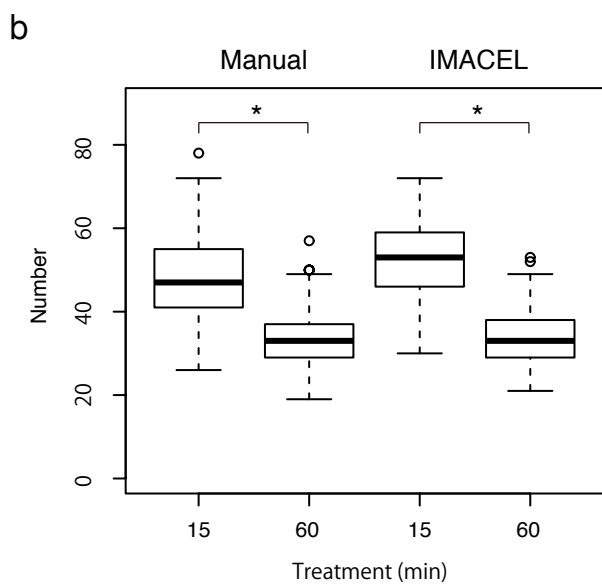
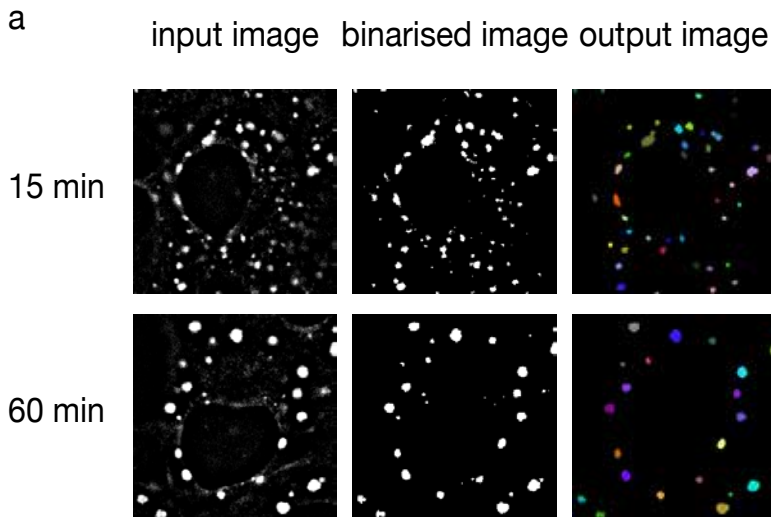


Figure 3. Results of the IMACEL particle analyser for extracting and evaluating stress granules in COS7 cells.

(a) Input image, binarised image, and output image of the IMACEL particle analyser. Comparison of the distribution of the number (b) and size (c) of stress granules against stress treating time evaluated using manual evaluation and IMACEL. Asterisks indicate significant differences (Mann–Whitney U test) between cells treated with 0.5 μ M sodium arsenite for 15 min and 60 min (in number: $p = 2.568 \times 10^{-13}$ and $p < 2.2 \times 10^{-16}$, in size: $p < 2.2 \times 10^{-16}$ and $p < 2.2 \times 10^{-16}$). (d) Total time spent on manual analysis versus the computational time of the IMACEL particle analyser. We measured 65 images each for specimen treated for 15 min and 60 min.

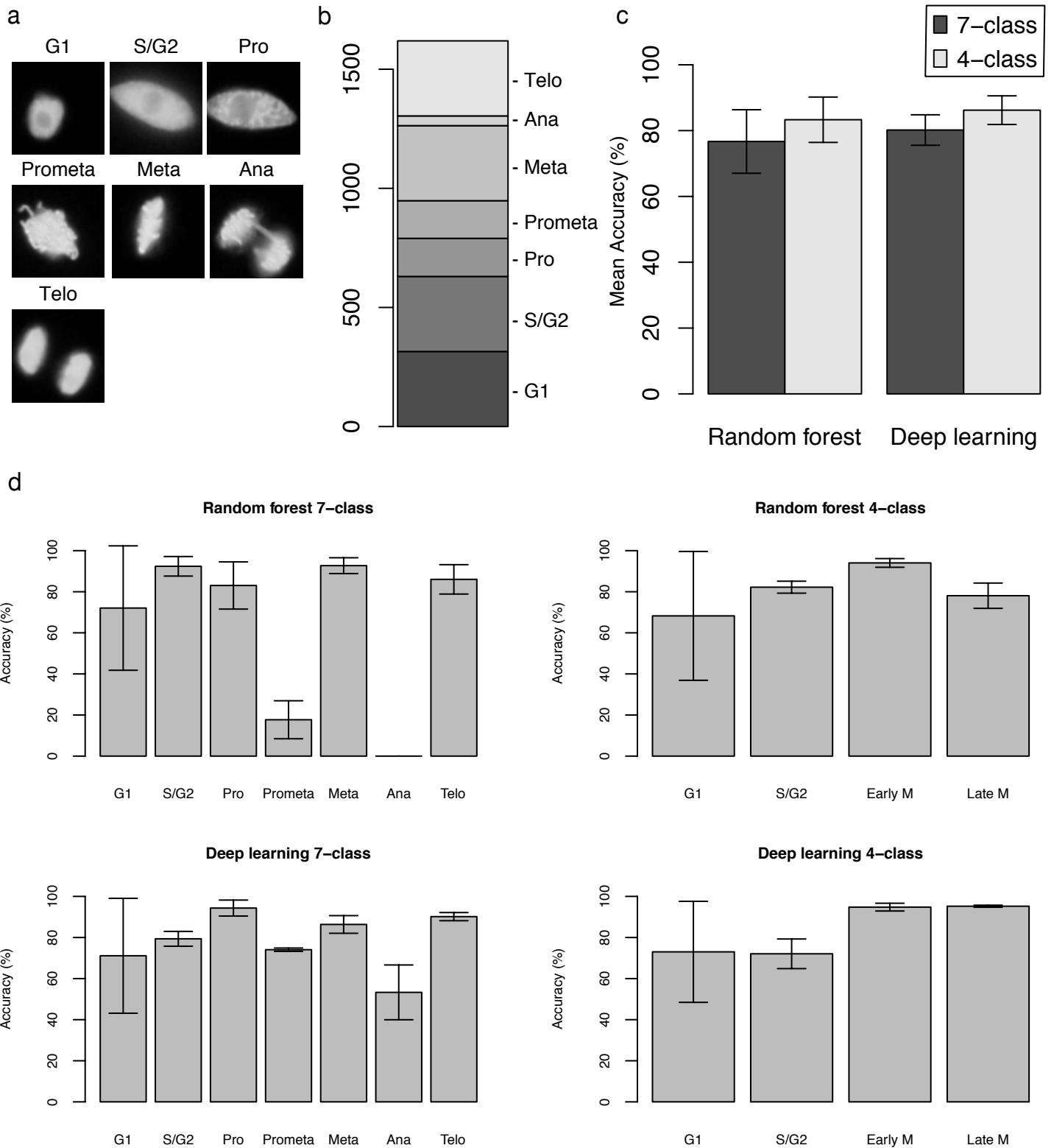
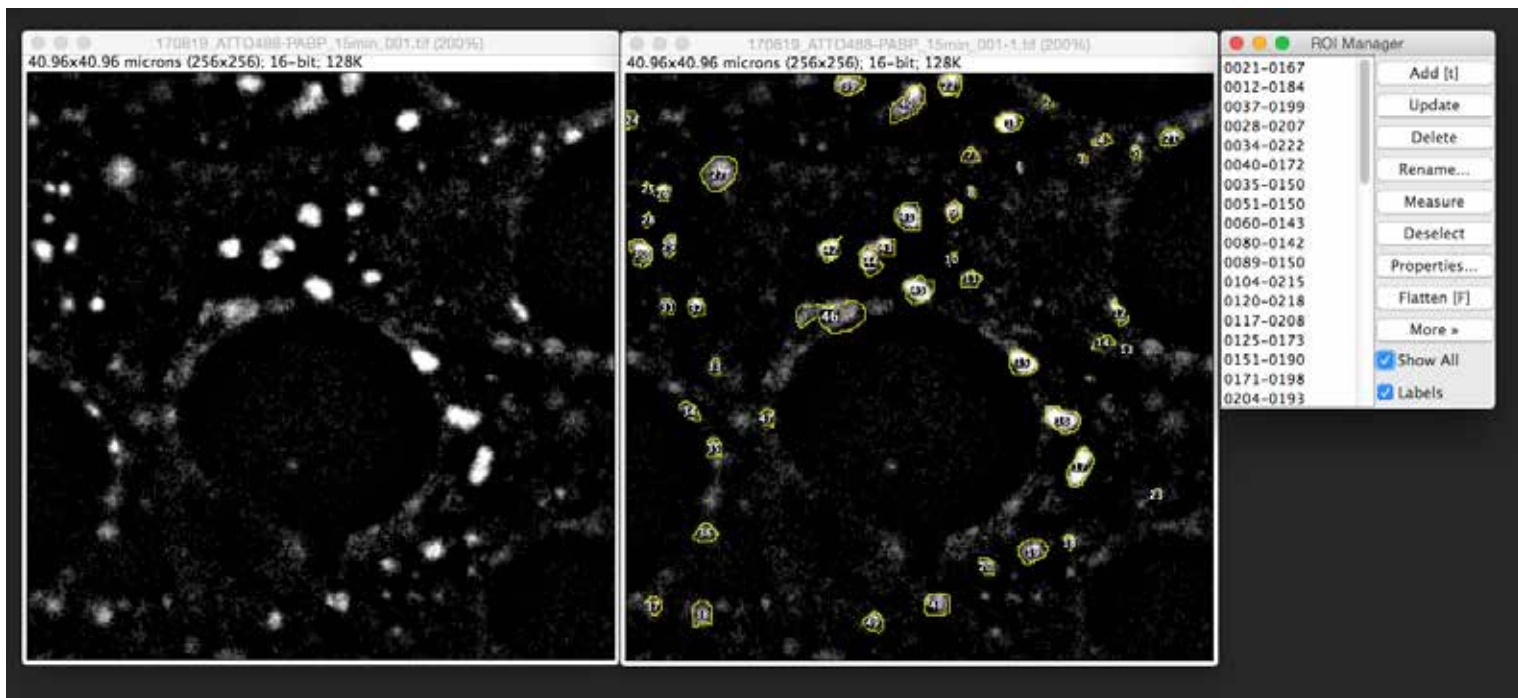
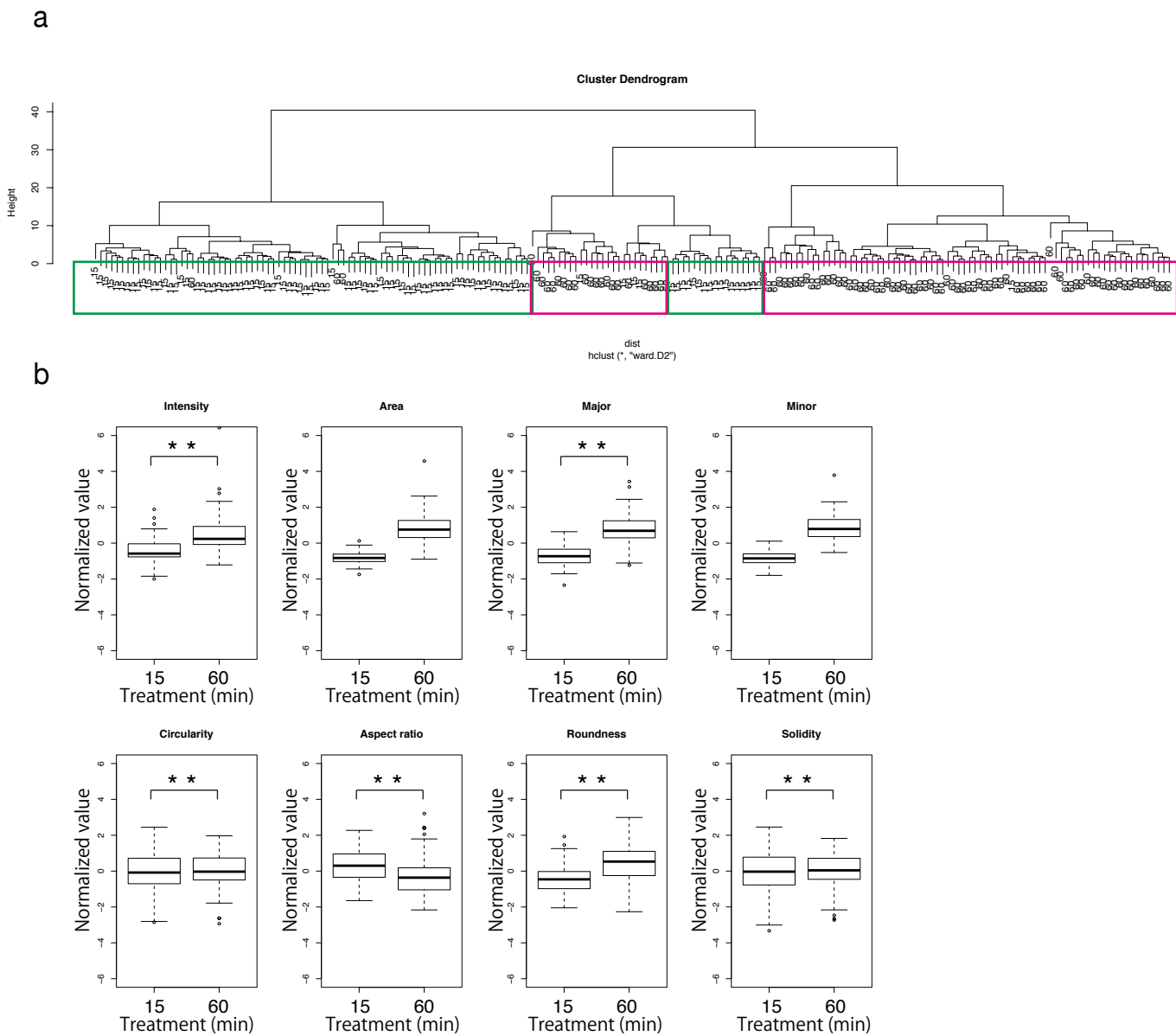


Figure 4 Results of the IMACEL classifier for cell cycle classification with nuclei visualised using fluorescent images.

(a) Representative images of each cell cycle in suspension-cultured plant cells. Nuclear regions were visualised using RFP-Histone H2B. (b) Distribution of the number of dataset images in each class. (c) Mean accuracy of cell cycle classification in seven-class and four-class classification using random forests and deep learning. For four-class classification, the prophase, prometaphase, and metaphase were integrated into the early mitotic phase. Anaphase and telophase were integrated into the late mitotic phase. (d) Accuracy of each cell cycle classification with bars representing the standard deviation based on three independent experiments.

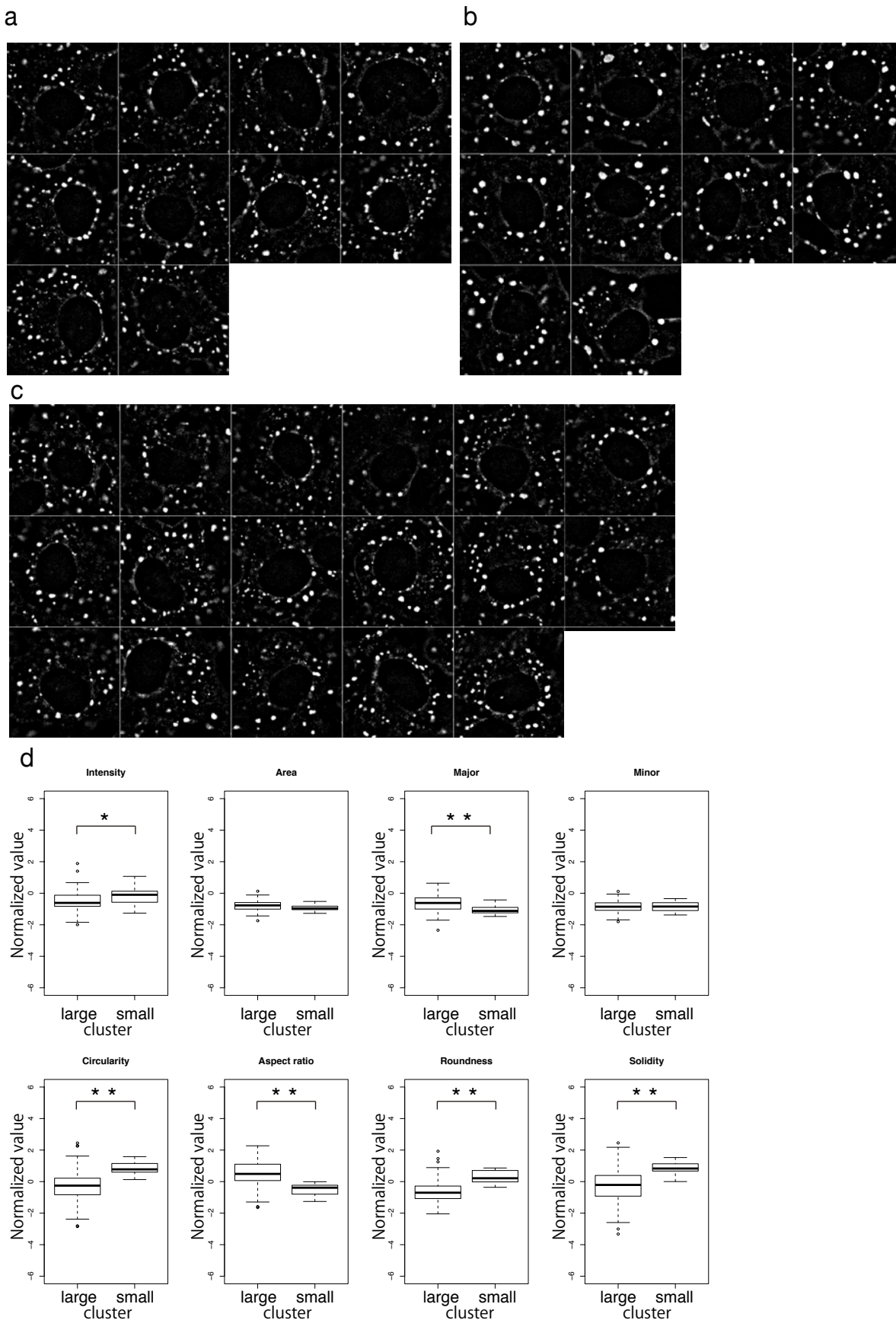


Supplemental Figure 1 Representative example of the manual evaluation of stress granules using ImageJ.



Supplemental Figure 2. Morphological analysis of stress granules using hierarchical clustering.

(a) Hierarchical clustering using ward method. Two large cluster was clearly organized by stress granules treated for 15 mins and 60 mins, although small cluster of stress granules treated for 15 mins was inserted in the cluster of 60 mins. Cluster generated by cells treated for 15 mins and 60 mins were indicated as green and magenta. (b) Comparison of morphological features of stress granules treated for 15 mins and 60 mins. Double asterisks indicate significant differences (Mann–Whitney U test, $P < 0.01$).



Supplemental Figure 3. Comparison of two different clusters within the 15-min treatment cells.

(a-b) Representative images of stress granules treated for 15 mins (a) and 60 mins (b). (c) Representative images of small cluster of stress granules treated for 15 mins revealed by clustering analysis. (d) Comparison of morphological features of large and small cluster of stress granules treated for 15 mins. Note that shape descriptors such as circularity and solidity were significantly different. Asterisk and double asterisks indicate significant differences (Mann-Whitney U test, $P < 0.05$, $P < 0.01$, respectively).

Supplemental Table 1 List of the implemented image processing methods in the IMACEL particle analyser.

1. Colour channel extraction
 1. Greyscale
 2. Red channel of RGB colour
 3. Green channel of RGB colour
 4. Blue channel of RGB colour
 5. Hue channel of HSV colour
 6. Saturation of HSV colours
2. Invert to black background
3. Removing excessive bright regions
 1. Skip this operation
 2. Median filtering of bright regions (radius = 5–21 pixels)
4. Shading
 1. Skip this operation
 2. Equalization of the global intensity histogram
 3. Equalization of the adaptive intensity histogram
5. Noise reduction
 1. Skip this operation
 2. Gaussian filtering (sigma = 1 - 4 pixel)
6. Edge enhancement
 1. Skip this operation
 2. Difference of Gaussian (sigma = 0.5, 4.0 or 0.5, 8.0)
7. Binarisation
 1. Threshold = 50
 2. Otsu method
 3. Adaptive Gaussian
 4. Adaptive Mean
 5. Edge extraction using the Canny method (threshold = 100, 200 or 10, 50)
8. Noise reduction using the closing method
 1. Skip this operation
 2. Closing (radius = 3–11 pixels)
9. Fill holes
 1. Skip this operation

2. Filling

10. Noise reduction using the opening method

1. Skip this operation

2. Opening (radius = 3–13 pixels)

11. Contour extraction

1. Simple segmentation

2. Dividing using watershed (blob ratio = 1%–15%)

Chapter 2

Quantitative evaluation of stromule frequency at hourly intervals in *Arabidopsis* stomatal guard cell chloroplasts

Introduction

In the previous chapter, I described the cell image analysis system IMACEL. Although the system is valuable for all cell image analyses, I examined whether it was possible to elucidate novel phenomena by analyzing the most complex intracellular structures. Consequently, I selected chloroplasts and organelles called stromules and proceeded with the analysis.

The chloroplast is one of several different types of plastid, all of which have common ancestral origins in photosynthetic cyanobacteria that are considered to have become organelles of eukaryotic cells by formation of intracellular symbioses. Compared with prokaryotic cells, chloroplasts appear to have acquired several new mechanisms related to the structure and specific functions of chloroplasts in plant cells. One mechanism is binary division of chloroplasts. Chloroplasts possess double membranes, and division of the inner membrane is achieved by means of the ancestral-type FtsZ ring, while the outer membranes divide by means of a complex of outer rings involving dynamin-related ARC5 (Chen *et al.* 2018). Another mechanism is chloroplast movement, termed chloroplast photorelocation, and involves cp-actin (Kadota *et al.* 2009, Suetsugu *et al.* 2010). Chloroplasts move within cells to accumulate in low light conditions or avoid high light conditions using

chloroplast-specific actin microfilaments, called cp-actin. Recent studies revealed involvement of cp-actin in photorelocation of nuclei to avoid high UV damage in *Arabidopsis* pavement cells (Higa *et al.* 2014, Suetsugu *et al.* 2016). A further mechanism is the occurrence of stromules.

Stromules are stroma-filled tubular structures that emerge from chloroplasts and other types of plastid. The direction of stromule protrusion is determined by three-way junction structures in the endoplasmic reticulum (Schattat *et al.* 2011) based on cytoskeletons (Kwok and Hanson 2004) and myosin motor proteins (Natesan *et al.* 2009). It has been reported that stromule formation is induced by salt or drought stress (Gray *et al.* 2012), treatment with sucrose or glucose (Schattat and Klosgen 2011) or strigolactones (Vismans *et al.* 2016), and by oxidation-reduction signals (Brunkard *et al.* 2015). Although stromules have roles in plant immunity (Caplan *et al.* 2015), little is known about other physiological functions of stromules or the significance of their formation, extent of protrusion and frequency of occurrence.

Previous studies examined the frequency of stromule formation during a diurnal cycle. The frequency of stromule formation increased in light conditions in pavement cells of young leaves of *Nicotiana benthamiana* (Brunkard *et al.* 2015) and in rosette leaves of 6-week-old *Arabidopsis* (Schattat *et al.* 2012, Barton *et al.* 2018). Although

Brunkard *et al.* reported that sucrose did not increase the frequency of stromule formation in *Arabidopsis* stomatal guard cells, the frequency of stromule formation in stomata is largely unknown (Brunkard *et al.* 2015).

In this study I performed detailed evaluation of stromule frequency in stomatal guard cells every hour during a diurnal cycle in developing and developed cotyledons of *Arabidopsis*. Quantitative evaluations revealed synchronized and periodic changes in stromule mean frequency in developing cotyledons. These results may shed light on the importance of stromule frequency and aid in investigations of the physiological roles of stromules.

Materials and methods

Plant materials

A transgenic line of *Arabidopsis thaliana*, stably expressing the transit peptide of AtFtsZ1-1 and yellow fluorescent protein (YFP) fusion protein under the control of the *CaMV35S* promoter, was established as previously described (Chen *et al.* 2009). *Arabidopsis* seeds were sterilized and grown on plates with 0.8% (w/v) agar, supplemented with half-strength Murashige and Skoog medium without sucrose, in a

growth chamber at 23.5°C with 12-h light and 12-h dark cycle or continuous light (100 $\mu\text{mol m}^{-2}\text{s}^{-1}$ white light). To compare different growth stages of the seedlings reliably, all of the seeds were placed on the growth medium at 1-h point of the light condition. Seeds were placed on the 12-h light and 12-h dark cycle (Fig. 5, 6) or continuous light (Fig. 8) for 72 h. Germinated seedlings were used for experiment as 1 day old seedling, and ungerminated seeds were removed from the growth medium and were not used in this study.

Cell staining

To visualize plasma membranes in the leaf cells, leaves were immersed in water supplemented with 32 μM *N*-(3-triethylammoniumpropyl)-4-(6-(4-(diethylamino)-phenyl)hexatrienyl)pyridinium dibromide (FM4-64; Molecular Probes, Invitrogen) for 10 min.

Microscope

To acquire confocal images, I used the inverted platform of a fluorescence microscope equipped with a confocal scanning unit (CSU X1, Yokogawa) and a cooled CCD camera (Cool-SNAP HQ, PhotoMetrics). Maximum intensity projection

images were reconstructed from serial optical sections with a 0.1- μm step size using METAMORPH software (Universal ImagingA). The images were processed digitally using ImageJ software.

Quantitative evaluation of stromule frequency and statistical analysis

Counting of stromule frequency in stomatal guard cell chloroplasts was performed by two researchers working independently using ImageJ software and all experimental images were evaluated both of the researchers. At least two seedlings were used for image acquisition at each time point. Stromule frequency was determined by manually counting the number of chloroplasts with or without stromules and expressed as the percentage of the total number of chloroplasts counted per stomata that had visible stromules. Mean values and standard errors were calculated for each time point using the numbers of samples as specified in the Figures. I used standard error, not standard deviation, as error bars in the Figures, similar to previous study reporting stromule frequency (Brunkard *et al.* 2015). To evaluate the significance of differences in the mean frequency of stromules, I used the Mann–Whitney U test, calculated using free statistical software R and RStudio (versions 3.3.1 and 1.1.383, respectively).

Results

Stromule frequency in light and dark conditions in *Arabidopsis* stomata

To examine the influence of a diurnal cycle on stromule frequency in stomatal guard cells I used seedlings of transgenic *Arabidopsis* that was stably expressing the transit peptide of AtFtsZ1-1 and YFP fusion protein under the control of the *CaMV35S* promoter (Chen *et al.* 2009). Seedlings were grown without sucrose to avoid induction of stromules by sucrose treatment, as reported in pavement cells and mesophyll cells (Schattat and Klosgen 2011), although Brunkard *et al.* (2015) reported that sucrose did not increase stromule formation in guard cells. I observed stomatal guard cell chloroplasts and counted the frequency of stromules in 1- and 2-day old cotyledons, taken as a developing leaf, and 5-day old cotyledons, as a developed leaf. Abnormal morphology of chloroplasts in stomata has not been reported in wild-type seedlings (Fujiwara *et al.* 2018) and I observed normal morphology of the chloroplasts in stomata and pavement cells in this study (Fig. 5a).

Quantitative evaluation of the frequency of stromules in stomata of 1-day old cotyledons during a diurnal cycle revealed that the mean frequency of stromules was significantly higher ($P = 0.0242$, Fig. 5b) in light than dark conditions, similar to the

results reported in *Arabidopsis* and *N. benthamiana* pavement cells (Schattat *et al.* 2012, Brunkard *et al.* 2015, Barton *et al.* 2018). However, I found no significant difference between light and dark conditions in 2-day old seedlings ($P = 0.2257$, Fig. 5b), and conversely, the mean stromule frequency was significantly higher in the dark period in 5-day old developed cotyledons ($P = 0.001557$, Fig. 5b). Unfortunately, significant differences were not observed in the result of IMACEL classifier (Fig. 5b). It may be because of not using 3D future value. These results suggest that the difference in frequency of stromules between light and dark conditions varied depending on the developmental stage of the cotyledon.

Detailed evaluation of stromule frequency at hourly intervals

To evaluate whether stromule frequency varied abruptly or gradually in the transition between light and dark conditions, I performed detailed observations of stromule frequency in *Arabidopsis* stomata at hourly intervals throughout the day in developing 1- and 2-day old seedlings and developed 5-day old seedlings. Surprisingly, quantitative evaluation revealed periodic increases and decreases in stromule mean frequency, with local peaks in frequency at 3–4-h intervals, independent of the developmental stage of the cotyledon, and similar results were

confirmed using manual evaluations (Fig. 6). Comparison of the periodic patterns in the developing cotyledons of 1- and 2-day-old seedlings revealed local peaks of stomule mean frequency at almost similar times (Fig. 6 a, b, d, e asterisks), although a synchronized periodic pattern was not apparent in the 5-day-old developed cotyledons (Fig. 6c, f). These results indicate that stomule mean frequency in stomata in developing *Arabidopsis* cotyledons was not constant but varied in an apparently synchronized and periodic pattern. Even under NaCl treatment conditions, it was confirmed that there is a rhythm every 2-4 hours in the occurrence frequency of stomules as in control (Fig. 7). It is suggested that the pathway for promoting stomule formation by NaCl addition and the pathway for increasing stomule formation frequency exist independently.

Effect of lighting conditions on the periodic patterns of stomule frequency

To evaluate whether the lighting conditions of 12 h light and 12 h dark affected the periodic pattern of stomule frequency, I quantified the stomule mean frequency every hour for 24 h in 1-day old seedlings that were grown in continuous light. I found that the periodic pattern of stomule mean frequency was also observed in continuous light (Fig. 8). These results suggest that the periodic pattern of stomule mean

frequency in *Arabidopsis* stomata was independent of the lighting conditions.

Discussion

Detailed evaluation of stomule mean frequency at hourly intervals during the diurnal cycle

In this study, I performed detailed observations of stomule frequency in *Arabidopsis* stomata at hourly intervals throughout the day, and quantitative evaluation revealed periodic patterns of stomule mean frequency. Previous studies, reporting that stomule frequency was increased in light conditions in *Arabidopsis* and *N. benthamiana* pavement cells, did not detect a periodic pattern of stomule frequency (Schattat *et al.* 2012, Brunkard *et al.* 2015, Barton *et al.* 2018). This may have been because of differences in the observational interval, as previous studies were performed at 2–4 h intervals. In my evaluation, re-analysis of all of the data every 1.5 or 2 h did not detect clear periodic patterns because some local peaks of stomule mean frequency were masked (data not shown). It may be necessary to observe stomule frequency using short intervals to detect rapid changes in frequency. Alternatively, it may be that periodic patterns of stomule mean frequency are specific to stomatal guard cells: I am currently investigating this possibility by evaluating

stromule frequency at short intervals in Arabidopsis pavement cells.

Synchronized and periodic patterns of stromule mean frequency in developing cotyledons

In this study, I reported two new findings. First, stromule frequency in Arabidopsis stomatal guard cells varied between light and dark conditions, depending on the developmental stage of the cotyledon (Fig. 5b–d). Second, stromule mean frequency showed periodic patterns. Two key features in these results lead to our hypothesis for the basis of periodic patterns of stromule mean frequency in Arabidopsis stomata:

1. Stromule frequency was periodic, with apparent local peaks in mean frequency at 3–4 h intervals, independent of the developmental stage of the cotyledon and of lighting conditions.

2. The periodic patterns of stromule mean frequency were almost synchronized during the diurnal cycle, at least in the developing cotyledons of 1- and 2-day old seedlings.

Although the periodic pattern of stromule mean frequency was not dependent on the light–dark cycle (Fig. 8), synchronization of the periodic pattern in developing

cotyledons was apparently dependent on lighting conditions, suggesting that the above two features of our results were maintained by at least two mechanisms. I suggest that a lighting condition-independent mechanism is involved in creating the periodic pattern of stomule mean frequency, while a lighting condition-dependent mechanism is involved in the synchronization of the periodic pattern during the diurnal cycle.

Stomule frequency in light and dark conditions

One of my new findings was that stomule frequency was higher in light conditions in 1-day old seedlings and in dark conditions in 5-day old seedlings (Fig. 5b, d). Obviously, these overall differences were composed of the sum of the short-term periodic patterns of stomule mean frequency. Stomata close and open from time to time, depending on the lighting conditions. It will be important to

determine whether the mechanisms of responding to lighting conditions and the closing and opening of stomata are related to stomule frequency.

Roles of periodic patterns of stomule frequency

The physiological roles of the periodic patterns of stomule mean frequency revealed in this study remain completely unknown. It has been reported that stomules were induced by the immune response to bacterial infection and were connected to nuclear defense signaling in *N. benthamiana* epidermal cells and mesophyll cells (Caplan *et al.* 2015). Therefore, there is a possibility that stomules may be required in epidermal cells ahead of rapid defense responses. However, constant production of stomules may be a waste of energy and so it may be that *Arabidopsis* guard cells have a mechanism that varies stomule frequency throughout the day and enables an efficient defense response.

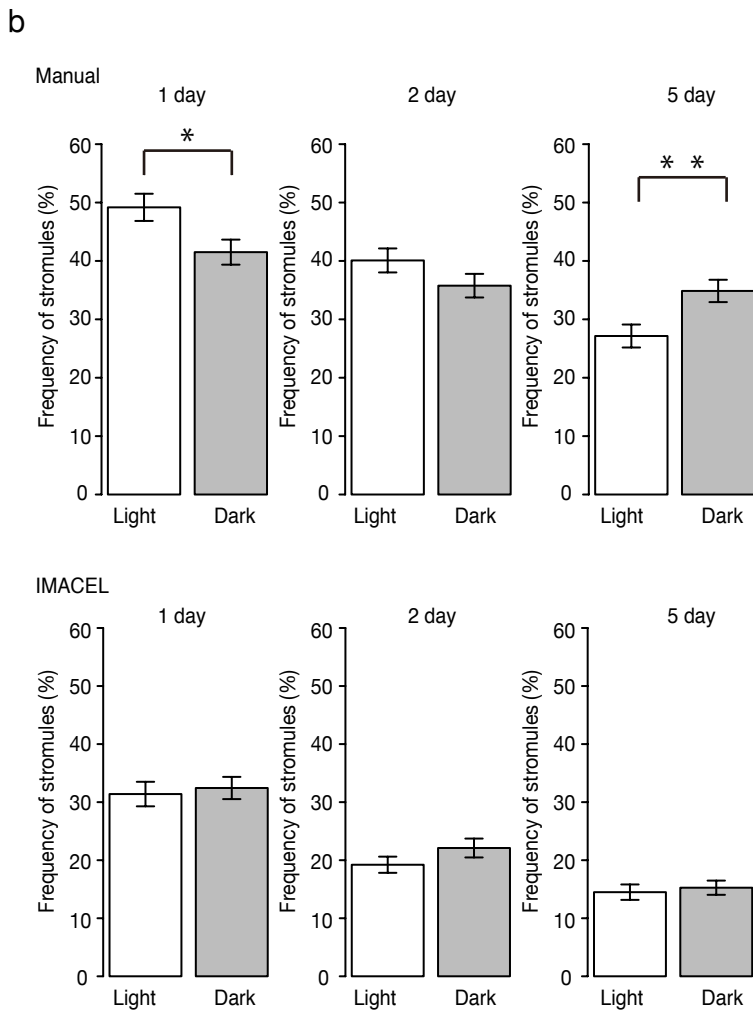
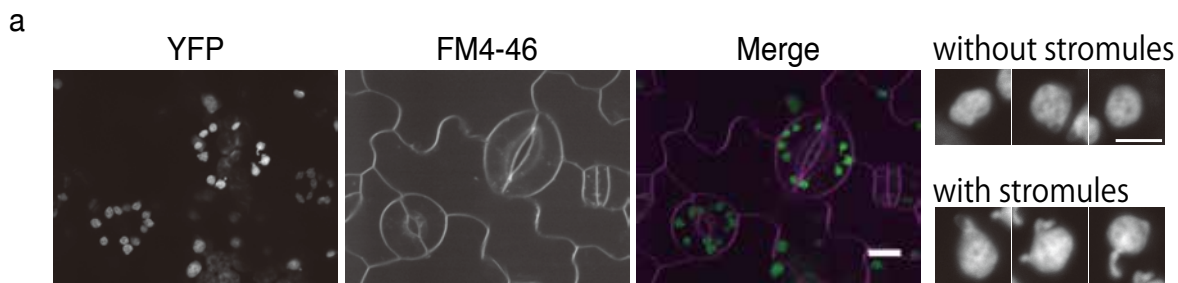


Figure 5. Representative images of chloroplasts with or without stromules and frequency of stromules in stomata of Arabidopsis seedlings of different ages.

(a) Chloroplasts visualized with YFP (left), plasma membrane visualized with FM4-64 (center) and merged image (right). Representative images of maximum intensity projections were constructed from serial optical sections with a 0.1- μm step size. Chloroplasts with and without stromules are shown in the enlarged images on the right. The scale bars in the merged image and enlarged image indicate 10 and 3 μm , respectively. (b) Frequency of stromules in stomatal guard cells of cotyledons grown in 12 h light and 12 h dark for 1 day, 2 days and 5 days then sampled during the light or dark periods (white and gray bars, respectively). Stromules were counted during a 1-h period for each time-point. I analyzed 5648–6170 plastids and at least 72 seedlings for each lighting condition, and the mean frequency of stromules (expressed as % of plastids with stromules) per stomata is shown. Error bars represent the standard error of 171–234 independent stomata. Asterisk and double asterisk indicate significant differences (U-test, $P = 0.0242$ and $P = 0.001557$, respectively) between mean stromule frequency in light and dark conditions.

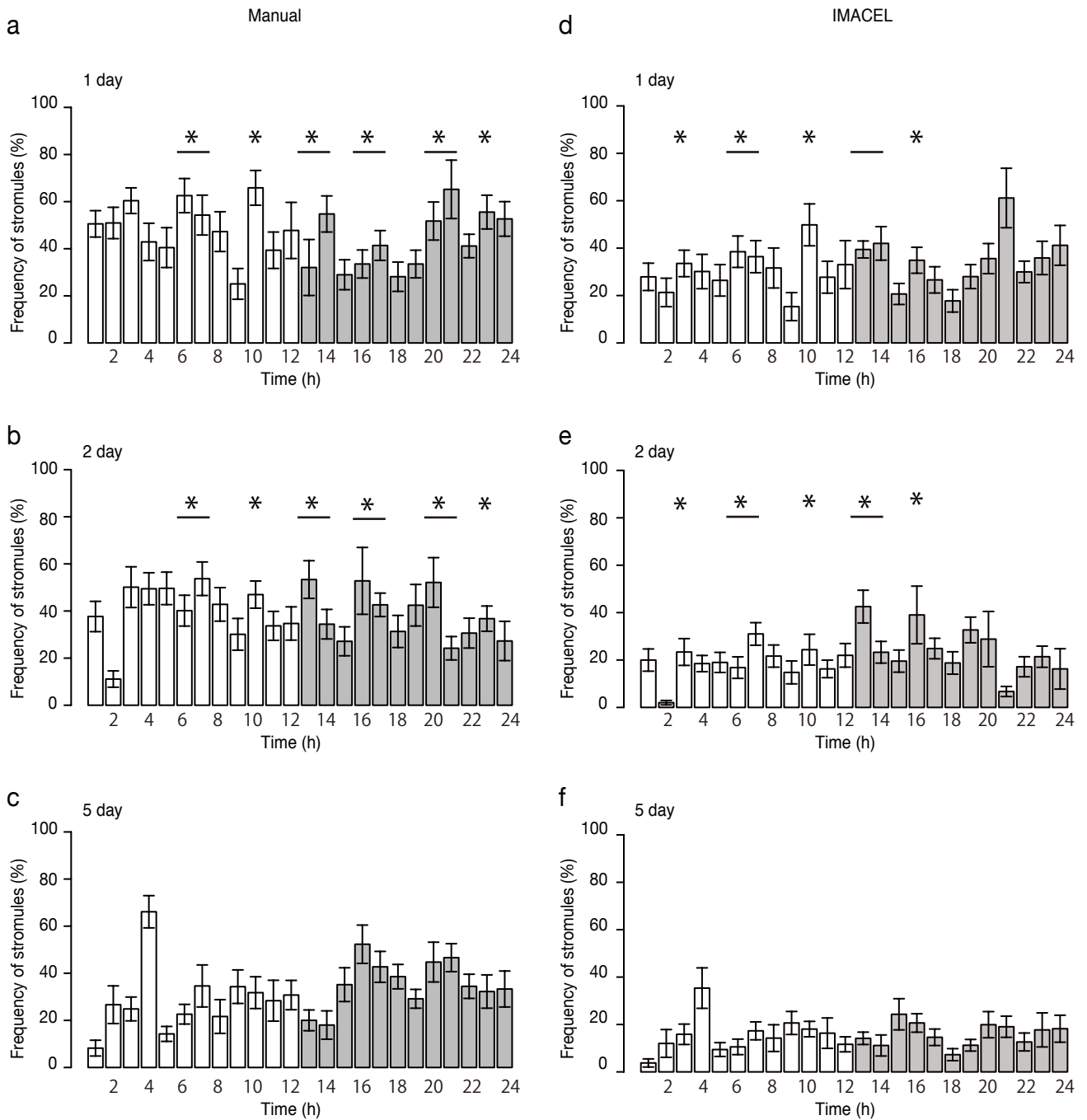


Figure 6. Mean frequency of stromules in stomata during a diurnal cycle in *Arabidopsis* seedlings of different ages. The mean frequency of stromules was counted in stomatal guard cells of cotyledons of *Arabidopsis* grown for 1 day (a, d), 2 days (b, e) and 5 days (c, f) with a 12 h light and 12 h dark cycle. White and gray bars indicate light and dark conditions, respectively. Counts of stromules were obtained at hourly time-points over 24 h. We analyzed 68–264 plastids and 2–3 seedlings at each time point, and the mean frequency of stromules (expressed as % of plastids with stromules) per stomata is shown. Error bars represent the standard error of 7–25 independent stomata. Asterisks indicate synchronized local peaks of stromule mean frequency in 1- and 2-day old seedlings.

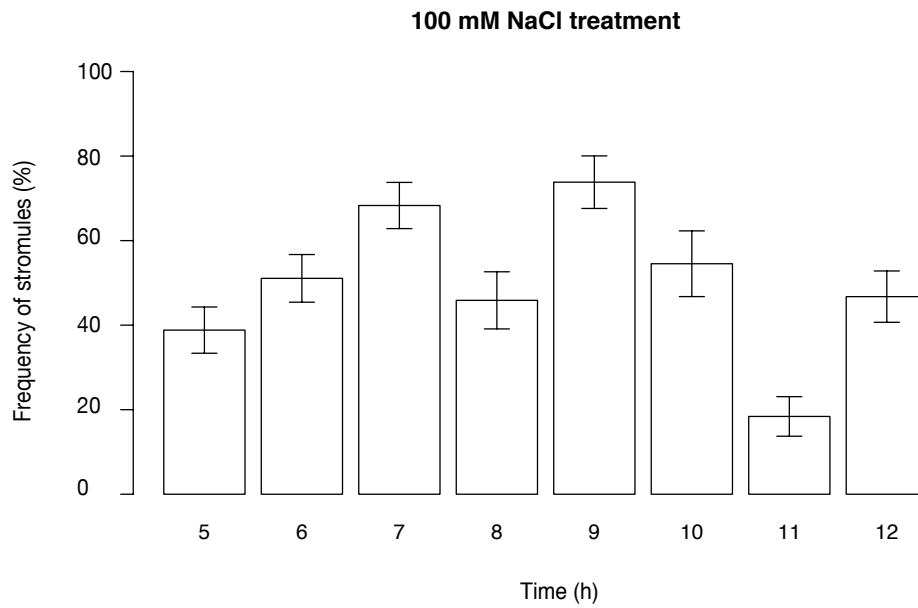


Figure 7. Mean frequency of stromules treated with 100 mM NaCl in stomata in Arabidopsis seedling. The mean frequency of stromules was counted in stomatal guard cells of cotyledons of Arabidopsis grown for 3 day. Counts of stromules were obtained at hourly time-points 5-12 h from light condition. We analyzed 92–222 plastids and 2–3 seedlings at each time point, and the mean frequency of stromules (expressed as % of plastids with stromules) per stomata is shown. Error bars represent the standard error of 10–27 independent stomata.

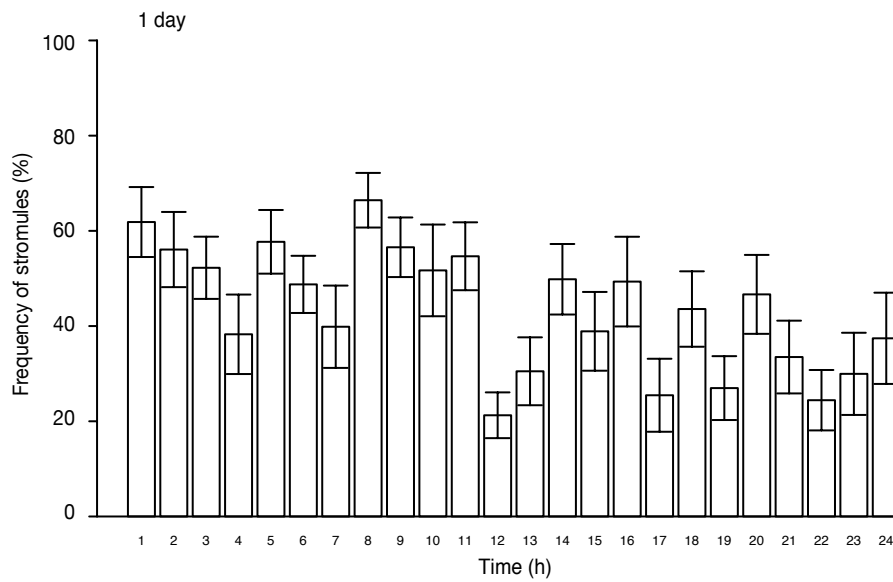


Figure 8. Mean frequency of stromules in stomata of *Arabidopsis* seedlings grown under continuous light. The frequency of stromules was counted at hourly time points in stomatal guard cells of cotyledons of 1-day old *Arabidopsis* seedlings grown under continuous light. We analyzed 96–283 plastids and 2 seedlings at each time point, and the mean frequency of stromules (expressed as % of plastids with stromules) per stomata is shown. Error bars represent the standard error of 10–26 independent stomata.

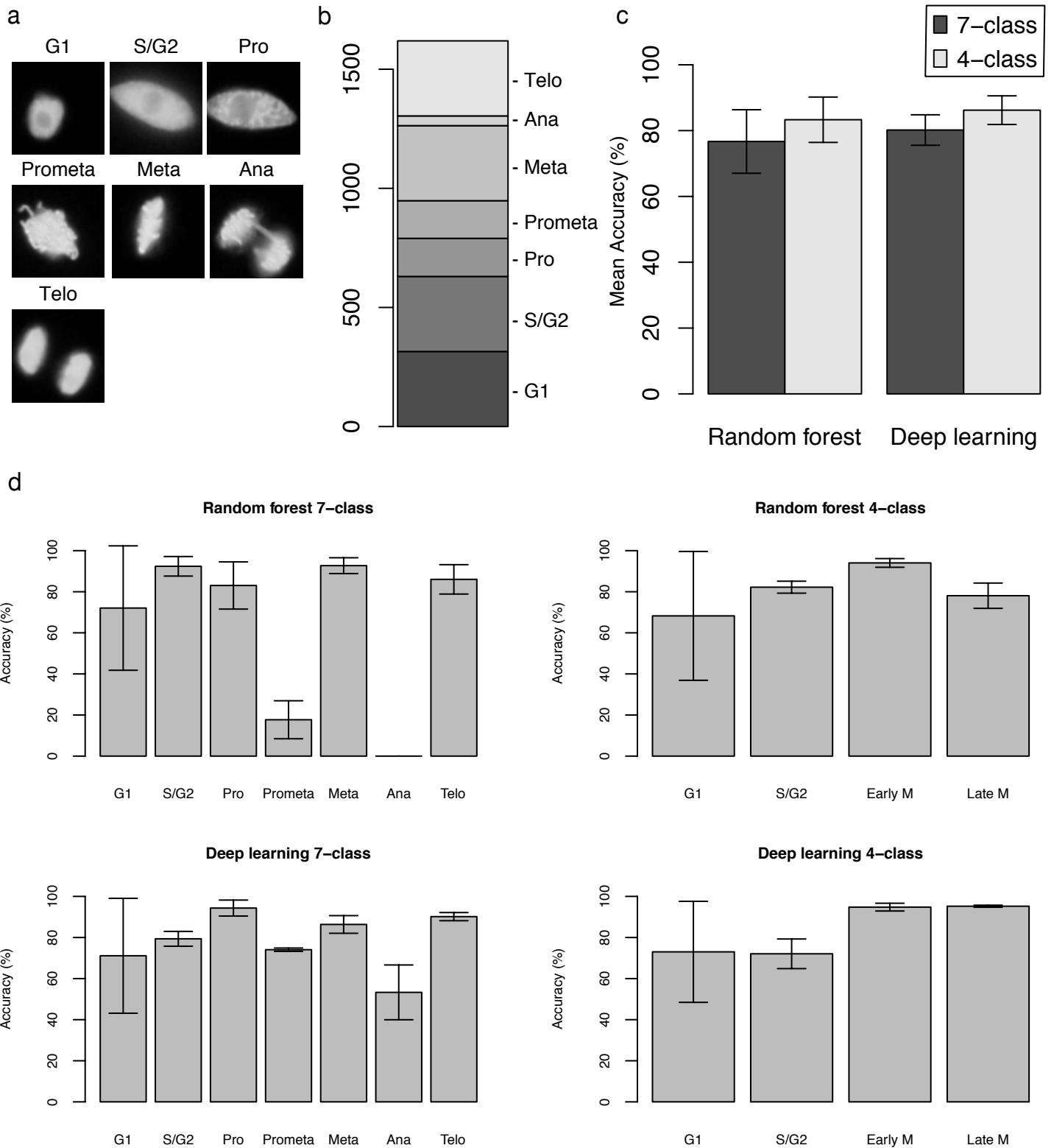
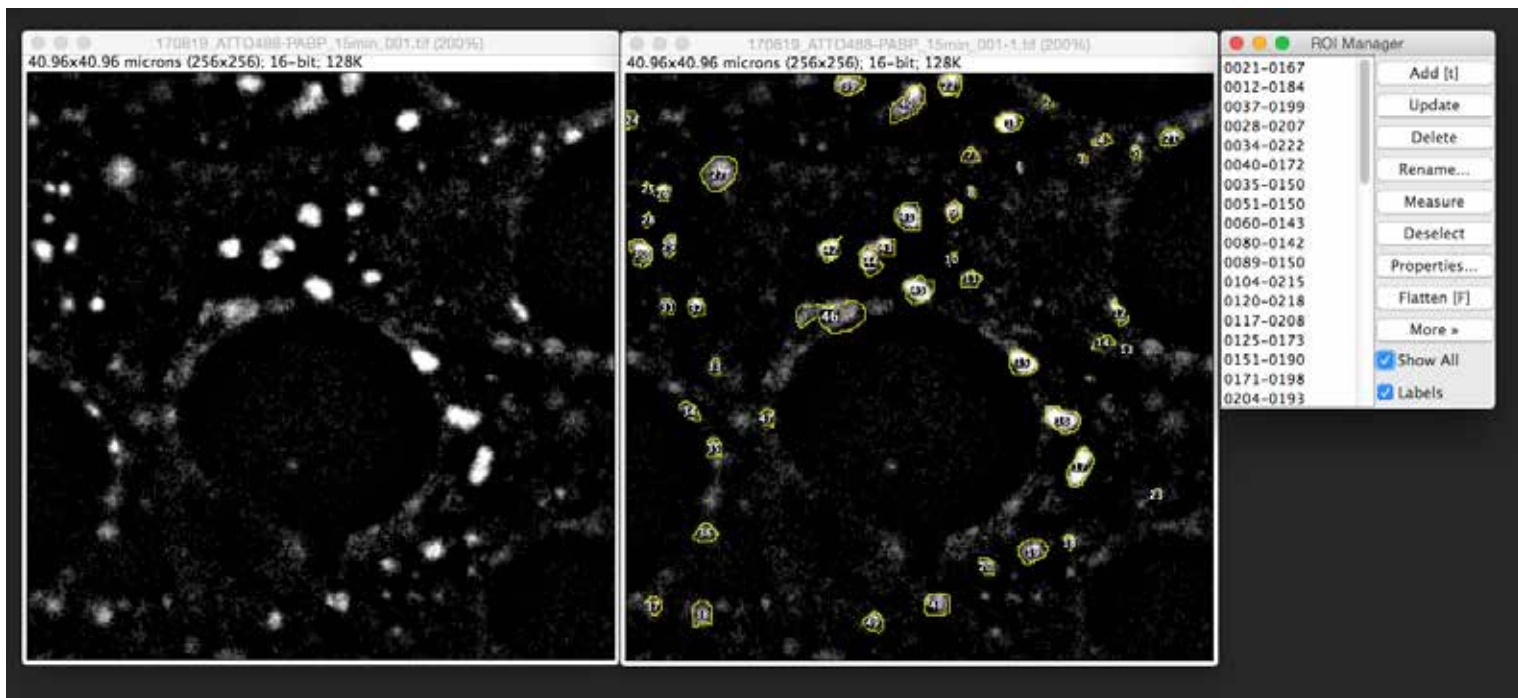


Figure 4 Results of the IMACEL classifier for cell cycle classification with nuclei visualised using fluorescent images.

(a) Representative images of each cell cycle in suspension-cultured plant cells. Nuclear regions were visualised using RFP-Histone H2B. (b) Distribution of the number of dataset images in each class. (c) Mean accuracy of cell cycle classification in seven-class and four-class classification using random forests and deep learning. For four-class classification, the prophase, prometaphase, and metaphase were integrated into the early mitotic phase. Anaphase and telophase were integrated into the late mitotic phase. (d) Accuracy of each cell cycle classification with bars representing the standard deviation based on three independent experiments.



Supplemental Figure 1 Representative example of the manual evaluation of stress granules using ImageJ.

Conclusion

In the present study, we developed IMACEL, a novel cellular image analysis system capable of efficiently analyzing large image data sets in the life sciences. Based on the components of the system, its novelty was acknowledged and a patent acquired. This tool facilitates the analysis of large sets of images rapidly and efficiently. In addition, we examined the stromule, which is a tubular structure protruding from the plastid of the plant cell. We demonstrated that there was a regular pattern in its frequency of appearance using IMACEL. Also, notably, it was revealed that there is a regular pattern even under salt stress conditions, which reportedly induces the appearance in stromules, and rhythm formation is an independent mechanism different from induction of stromal emergence under salt stress.

I aim to employ IMACEL in numerous types of research and contribute to the advancement of life sciences. In addition, although novel findings were presented regarding the occurrence frequency of stromules, I aim to analyse large data sets using IMACEL in the future to elucidate more detailed functions.

References

- Barton, K. A., Wozny, M. R., Mathur, N., Jaipargas, E. A. and Mathur, J. 2018. Chloroplast behaviour and interactions with other organelles in *Arabidopsis thaliana* pavement cells. *J. Cell Sci.* 131: jcs202275.
- Brunkard, J. O., Runkel, A. M. and Zambryski, P. C. 2015. Chloroplasts extend stromules independently and in response to internal redox signals. *Proc. Natl. Acad. Sci. USA* 112: 10044–10049.
- Buades A, Coll B, Morel J-M. A Non-Local Algorithm for Image Denoising. In: *CVPR 2005: Proceedings of the IEEE Computer Society Conference on Computer Vision and Pattern Recognition*; 2005 Jun 20; Washington DC, USA. IEEE Computer Society; 2005. p. 60-5. doi:10.1109/CVPR.2005.38
- Caplan, J. L., Kumar, A. S., Park, E., Padmanabhan, M. S., Hoban, K., Modla, S., Czymmek, K. and Dinesh-Kumar, S. P. 2015. Chloroplast stromules function during innate immunity. *Dev. Cell* 34: 45–57.
- Chang CC, Lin CJ. LIBSVM: A library for support vector machines. *ACM Trans Intell Syst Technol.* 2011 Apr;2(3):1-27. doi:10.1145/1961189.1961199.
- Chen, C., MacCready, J. S., Ducat, D. C. and Osteryoung, K. W. 2018. The molecular machinery of chloroplast division. *Plant Physiol.* 176: 138–151.
- Chen, Y., Asano, T., Fujiwara, M. T., Yoshida, S., Machida, Y. and Yoshioka, Y. 2009. Plant cells without detectable plastids are generated in the crumpled leaf mutant of *Arabidopsis thaliana*. *Plant Cell Physiol.* 50: 956–969.
- Chessel A. An overview of data science uses in bioimage informatics. *Methods* 2017 Feb;115:110-8. doi:10.1016/j.ymeth.2016.12.014.
- Collier NC, Schlesinger MJ. The dynamic state of heat shock proteins in chicken embryo fibroblasts. *J Cell Biol.* 1986 Oct;103(4):1495-507.

Danuser G. Computer vision in cell biology. *Cell*. 2011 Nov;147(5):973-8. doi:10.1016/j.cell.2011.11.001.

Eulenberg P, Köhler N, Blasi T, Filby A, Carpenter AE, Rees P, et al. Reconstructing cell cycle and disease progression using deep learning. *Nat Commun*. 2017 Sep;8(1):463. doi:10.1038/s41467-017-00623-3.

Fujiwara, M. T., Yasuzawa, M., Kojo, K. H., Niwa, Y., Abe, T., Yoshida, S., Nakano, T. and Itoh, R. D. 2018. The Arabidopsis *arc5* and *arc6* mutations differentially affect plastid morphology in pavement and guard cells in the leaf epidermis. *PLoS One* 13: e0192380.

Gray, J. C., Hansen, M. R., Shaw, D. J., Graham, K., Dale, R., Smallman, P., Natesan, S. K. and Newell, C. A. 2012. Plastid stromules are induced by stress treatments acting through abscisic acid. *Plant J*. 69: 387–398.

Hayashi T, Sano T, Kutsuna N, Kumagai-Sano F, Hasezawa S. Contribution of anaphase B to chromosome separation in higher plant cells estimated by image processing. *Plant Cell Physiol*. 2007 Oct;48(10):1509-13. doi:10.1093/pcp/pcm117.

Higa, T., Suetsugu, N., Kong, S. G. and Wada, M. 2014. Actin-dependent plastid movement is required for motive force generation in directional nuclear movement in plants. *Proc. Natl. Acad. Sci. USA* 111: 4327–4331.

Kadota, A., Yamada, N., Suetsugu, N., Hirose, M., Saito, C., Shoda, K., Ichikawa, S., Kagawa, T., Nakano, A. and Wada, M. 2009. Short actin-based mechanism for light-directed chloroplast movement in Arabidopsis. *Proc. Natl. Acad. Sci. USA* 106: 13106–13111.

Kamatani T, Fukunaga K, Miyata K, Shirasaki Y, Tanaka J, Baba R, et al. Construction of a system using a deep learning algorithm to count cell numbers in nanoliter wells for viable single-cell experiments. *Sci Rep*. 2017 Dec;7(1):16831. doi:10.1038/s41598-017-17012-x.

Krizhevsky A, Sutskever I, Hinton GE. Imagenet classification with deep convolutional neural networks. In: Pereira F, Burges CJC, Bottou L, Weinberger KQ, editors. *Advances in Neural Information Processing Systems 25*. Curran Associates; 2012. p. 1097-105.

Kumagai-Sano F, Hayashi T, Sano T, Hasezawa S. Cell cycle synchronization of tobacco BY-2 cells. *Nat Protoc*. 2006 Dec;1(6):2621-7. doi:10.1038/nprot.2006.381.

Kutsuna N, Higaki T, Matsunaga S, Otsuki T, Yamaguchi M, Fujii H, et al. Active learning framework with iterative clustering for bioimage classification. *Nat Commun*. 2012 Aug;3:1032. doi:10.1038/ncomms2030.

Kwok, E. Y. and Hanson, M. R. 2004. In vivo analysis of interactions between GFP-labeled microfilaments and plastid stromules. *BMC Plant Biol*. 4: 2.

Nagata T, Nemoto Y & Hasezawa S. Tobacco BY-2 cell line as the 'HeLa' cell in the cell biology of higher plants. *Int Rev Cytol*. 1992 Jan 1;132, 1-30.

Natesan, S. K., Sullivan, J. A. and Gray, J. C. 2009. Myosin XI is required for actin-associated movement of plastid stromules. *Mol. Plant* 2: 1262–1272.

Nover L, Scharf KD, Neumann D. Cytoplasmic heat shock granules are formed from precursor particles and are associated with a specific set of mRNAs. *Mol Cell Biol*. 1989 Mar;9(3):1298-308.

Nover L, Scharf KD, Neumann D. Formation of cytoplasmic heat shock granules in tomato cell cultures and leaves. *Mol Cell Biol*. 1983 Sep;3(9):1648-55.

Peng H, Zhou J, Zhou Z, Bria A, Li Y, Kleissas DM, et al. Bioimage Informatics for Big Data. In: De Vos W., Munck S., Timmermans JP, editors. *Focus on Bio-Image Informatics*. *Advances in Anatomy, Embryology and Cell Biology*. Cham: Springer; 2016. pp. 263-72, doi:10.1007/978-3-319-28549-8_10.

Rueden CT, Schindelin J, Hiner MC, DeZonia BE, Walter AE, Arena ET, et al. ImageJ2: ImageJ for the next generation of scientific image data. *BMC Bioinformatics*. 2017 Dec;18(1):529. doi:10.1186/s12859-017-1934-z.

Sasaki N, Ishiwata T, Hasegawa F, Michishita M, Kawai H, Matsuda Y, et al. Stemness and anti-cancer drug resistance in ATP-binding cassette subfamily G member 2 highly expressed pancreatic cancer is induced in 3D culture conditions. *Cancer Sci*. 2018 Apr;109(4):1135-46. doi:10.1111/cas.13533

Schattat, M. H., Barton, K., Baudisch, B., Klosgen, R. B. and Mathur, J. 2011. Plastid stromule branching coincides with contiguous endoplasmic reticulum dynamics. *Plant Physiol*. 155: 1667–1677.

Schattat, M. H. and Klosgen, R. B. 2011. Induction of stromule formation by extracellular sucrose and glucose in epidermal leaf tissue of *Arabidopsis thaliana*. *BMC Plant Biol*. 11: 115.

Settles B. Active Learning literature survey. Madison (WI): University of Wisconsin; 2009 Report No.: 1648. Available from: <http://axon.cs.byu.edu/~martinez/classes/778/Papers/settles.activelearning.pdf>

Sommer C., Gerlich DW. Sommer C, Gerlich DW. Machine learning in cell biology – teaching computers to recognize phenotypes. *J Cell Sci*. 2013 Dec;126(24):5529-39. doi:10.1242/jcs.123604.

Schattat, M. H., Klosgen, R. B. and Mathur, J. 2012. New insights on stromules: stroma filled tubules extended by independent plastids. *Plant Signal. Behav*. 7: 1132–1137.

Suetsugu, N., Higa, T., Gotoh, E. and Wada, M. 2016. Light-induced movements of chloroplasts and nuclei are regulated in both cp-actin-filament-dependent and -independent manners in *Arabidopsis thaliana*. *PLoS One* 11: e0157429.

Suetsugu, N., Yamada, N., Kagawa, T., Yonekura, H., Uyeda, T. Q., Kadota, A. and Wada, M. 2010. Two kinesin-like proteins mediate actin-based chloroplast movement in *Arabidopsis thaliana*. *Proc. Natl. Acad. Sci. USA* 107: 8860–8865.

Vismans, G., van der Meer, T., Langevoort, O., Schreuder, M., Bouwmeester, H., Peisker, H., Dorman, P., Ketelaar, T. and van der Krol, A. 2016. Low-phosphate induction of plastidal stromules is dependent on strigolactones but not on the canonical strigolactone signaling component MAX2. *Plant Physiol.* 172: 2235–2244.